Lab on a Chip

Cite this: *Lab Chip*, 2012, **12**, 1533

www.rsc.org/loc

PAPER

Integration of field effect transistor-based biosensors with a digital microfluidic device for a lab-on-a-chip application†

Kyungyong Choi,[a] Jee-Yeon Kim,[a] Jae-Hyuk Ahn,[a] Ji-Min Choi,[a] Maesoon Im[b] and Yang-Kyu Choi*[a]

Received 4th December 2011, Accepted 3rd February 2012
DOI: 10.1039/c2lc21203j

A new platform for lab-on-a-chip system is suggested that utilizes a biosensor array embedded in a digital microfluidic device. With field effect transistor (FET)-based biosensors embedded in the middle of droplet-driving electrodes, the proposed digital microfluidic device can electrically detect avian influenza antibody (anti-AI) in real time by tracing the drain current of the FET-based biosensor without a labeling process. Digitized transport of a target droplet enclosing anti-AI from an inlet to the embedded sensor is enabled by the actuation of electrowetting-on-dielectrics (EWOD). A reduction of the drain current is observed when the target droplet is merged with a pre-existing droplet on the embedded sensor. This reduction of the drain current is attributed to the specific binding of the antigen and the antibody of the AI. The proposed hybrid device consisting of the FET-based sensor and an EWOD device, built on a coplanar substrate by monolithic integration, is fully compatible with current fabrication technology for control and read-out circuitry. Such a completely electrical manner of inducing the transport of bio-molecules, the detection of bio-molecules, the recording of signals, signal processing, and the data transmission process does not require a pump, a fluidic channel, or a bulky transducer. Thus, the proposed platform can contribute to the construction of an all-in-one chip.

1. Introduction

Digital microfluidics is now being focused on as a core technology for lab-on-a-chip devices due to the ability of this technology to manipulate picolitre-to-microlitre-sized droplets with a set of several operations.[1,2] In digital microfluidic devices, discrete droplets are manipulated by applying an electrical field to the droplets *via* an array of electrodes. In contrast to microfluidic channels where a continuous flow of fluids occurs, each sample and reagent are individually addressable by discrete droplets, which facilitates exquisite control over chemical reactions. Most fluidic operations, such as creating, transporting, cutting and merging, can be carried out on digital microfluidic devices using discrete droplets rather than the conventional continuous flow of liquids in the microfluidic channels.[3] With the ability to control discrete droplets, digital microfluidic devices have demonstrated biological experiments such as enzymatic glucose assays on human physiological fluids,[4] proteomic sample purification,[5] polymerase chain reactions[6] and cell culturing[7] on chips.

Many research groups have focused on the development of digital microfluidic devices that automatically conduct biological or chemical experiments on chips while only consuming a relatively small amount of the sample and with less required effort.[1,2] However, for a lab-on-a-chip platform, a digital microfluidic device combined with a sensor part capable of analyzing a target material is required. Therefore, many attempts have been made to integrate these components.[8] UV/Vis spectroscopy has been used for the detection of a target material due to its capability to diagnose the absorbance characteristics of a material.[4] The coupling of a digital microfluidic device to surface plasmon resonance (SPR) imaging has also been attempted.[9,10] Samples have been analyzed using matrix-assisted laser desorption/ionization mass spectrometry (MALDI-MS).[5,11–13] Because these approaches require a bulky transducer and an analysis tool, they are not ideal for the all-in-one-chip platform that carries out processes ranging from liquid manipulation *via* detection to data acquisition.

Although previous studies have involved many types of microfluidic experiments using digital microfluidic devices, both real-time and on-chip measurements are not easy tasks.[4,5,9,11–13] Therefore, there is at present a strong push to realize real-time, on-chip measurements and to combine a digital microfluidic device and a sensor on a single chip, especially as a means of downsizing the lab-on-a-chip design.[8]

On the other hand, sensors based on field effect transistors (FETs) have rapidly developed owing to their inherent advantage of a small size and feasibility for label-free chip-based detection

[a]*Department of Electrical Engineering, KAIST, Daejeon, 305-701, Republic of Korea. E-mail: ykchoi@ee.kaist.ac.kr; Fax: +82-42-350-8565; Tel: +82-42-350-3477*
[b]*Department of Neurosurgery, Massachusetts General Hospital, Harvard Medical School, Boston, MA 02114, USA*

† Electronic supplementary information (ESI) available: Further description of fabricational and experimental steps and movie clips of droplet actuations are available. See DOI: 10.1039/c2lc21203j

compared to other types of biosensors.[14–19] In FETs, current flows through an electrical path called a channel between a source and a drain. The conductivity of the channel can be controlled by external factors such as bias to a gate of the FET or charged molecules adsorbed near the channel. FET-based biosensors detect bio-molecules by tracing a change in the current caused by specific effects arising from the bio-molecules. By functionalizing the biosensor surface with molecules that specifically bind to the target molecules, the target bio-molecules can easily be detected without the requirement of a bulky transducer to convert the binding signature from a bio- or chemical signal to an electrical signal for a chip-based analysis. In other words, the FET itself is the transducer because the characteristics of the FET are electrically modulated by the changes in the dielectric constant and surface charge that arise from the target bio-molecules.

Herein, we report the hybrid integration of a biosensor termed the underlap FET[20] and a digital microfluidic device to realize a lab-on-a-chip platform. With the proposed device, it is possible to transport a droplet enclosing target bio-molecules and to detect the target molecules in real time on a single chip. As proof of concept, the antibody of the avian influenza virus (anti-AI) is electrically detected without a labeling process in real time.

2. Experimental methods

2.1 Device design and working principle

To implement a digital microfluidic device with biosensors on a single chip, the sensor part, *i.e.*, the underlap FETs, is initially fabricated because FETs require a few high-temperature processes above 900 °C. Thereafter, the digital microfluidic parts are integrated over an inter-layer dielectric (ILD) consisting of a silicon dioxide for isolation between the sensor and the digital fluidic device. A top view of the proposed device schematic is shown in Fig. 1(a). The figure shows the droplet-driving electrodes used for the digital microfluidic operation. Biosensors are buried under the droplet-driving electrodes. On top of these electrodes, dielectric layers composed of silicon dioxide, silicon nitride and CYTOP™ (Asahi Glass Company, Japan) are sequentially deposited and patterned for the EWOD actuation (see the ESI document†). As shown in Fig. 1(b), opening holes are made through the ILD through which a target droplet comes into contact with the sensing area of the underlap FET. When target bio-molecules are bound to pre-existing probe molecules in the sensing area, additional surface charges are induced. Thus, the FET characteristics change and the specific binding can be electrically sensed by tracing these changes.

2.1.1 Underlap FET biosensor. A conventional metal-oxide-semiconductor field effect transistor (MOSFET) is comprised of a source and a drain connected by a silicon channel. A gate, electrically insulated by gate oxide above the channel, controls the current flowing from the drain to the source. There are two types of MOSFETs: n-channel and p-channel devices. In this experiment, n-channel devices are used. In this case, a very small fraction of the source and drain junction is overlapped with the gate. In contrast, the underlap FET device is a special type of FET that relies on an open sensing area termed the "underlap region" between the gate and the drain, as shown in Fig. 1(c) and (d). This underlap region provides a binding site for bio-molecules which allows the underlap FET device to function as a biosensor. Fabrication details for the underlap FETs are available in the literature.[20] In this experiment, the range of the underlap length was from 300 nm to 1200 nm. Before the detection of the anti-AI (Peptron (Korea)) in the droplet, the antigen of the avian influenza virus (AIa), which is linked with the silica-binding proteins (SBPs) at one end (thus simply referred to as SBP-AIa), is immobilized on the underlap region.[17]

The specific binding of the anti-AI and the surface-immobilized SBP-AIa leads to a reduction in the drain current (I_D) in the n-channel underlap FET because the negative charges of the anti-AI suppress the creation of inverted charges, which are the major carriers that create the I_D. In contrast, the I_D of the underlap FET is scarcely affected by the addition of anti-rabbit whole immunoglobulin G (anti-rabbit IgG, Sigma-Aldrich), which has the characteristic of non-specificity against the SBP-AIa.

2.1.2 Digital microfluidic device. As shown in Fig. 2(a), the underlap FETs were initially placed in the middle of the droplet-driving electrodes of the digital microfluidic device. The digital microfluidic device was fabricated on top of the ILD over the underlap FETs. Silicon dioxide of a thickness of 200 nm (ILD) was then deposited on the underlap FETs by a low-pressure chemical vapor deposition (LPCVD) process to isolate the digital microfluidic device from the underlap FETs. Afterwards, contact holes were patterned through the ILD by photo-lithography and subsequent wet etching with hydrofluoric acid (HF) to create the interconnections between the localized gate, source, and drain and the corresponding large probe pad. *In situ* n^+-doped polycrystalline silicon (poly-Si) with a thickness of 200 nm was deposited by LPCVD, thus filling the contact holes. This was then patterned by photo-lithography and reactive ion etching. This poly-Si was used for the probing pads, the droplet-driving electrodes, and the pre-charging electrode of the digital microfluidic device. It should be noted that the probing pads were placed outside the droplet-moving region and were interconnected by the poly-Si lines to apply voltage to the electrodes so as to avoid electrolysis during the transport of a water droplet by EWOD actuation, as shown in Fig. 2(b) and (c). Afterwards, all of the poly-Si patterns were shielded by silicon dioxide with a thickness of 50 nm and silicon nitride with a thickness of 150 nm, which were sequentially deposited by LPCVD for the prevention of electrical shorts between the driving electrodes and the water droplet during the EWOD actuation. The passivation layer of the silicon dioxide (50 nm) and the silicon nitride (150 nm) was patterned by photo-lithography and reactive ion etching to open several regions on the probing pads, the droplet-driving electrodes, and the pre-charging electrode for electrical biasing. The underlying ILD on the underlap FETs was additionally etched by HF until the underlap region accommodating the bio-molecules was exposed (holes in Fig. 2(b) and (c)). Meanwhile, the opened poly-Si pads were not etched by virtue of infinite selectivity of the poly-Si against HF. In addition, re-oxidation was carried out at 700 °C for 30 minutes to form a thin oxide (~5 nm) layer on the underlapped silicon surface. This thin oxide serves not only as a binding site for SBP-AIa molecules but also as

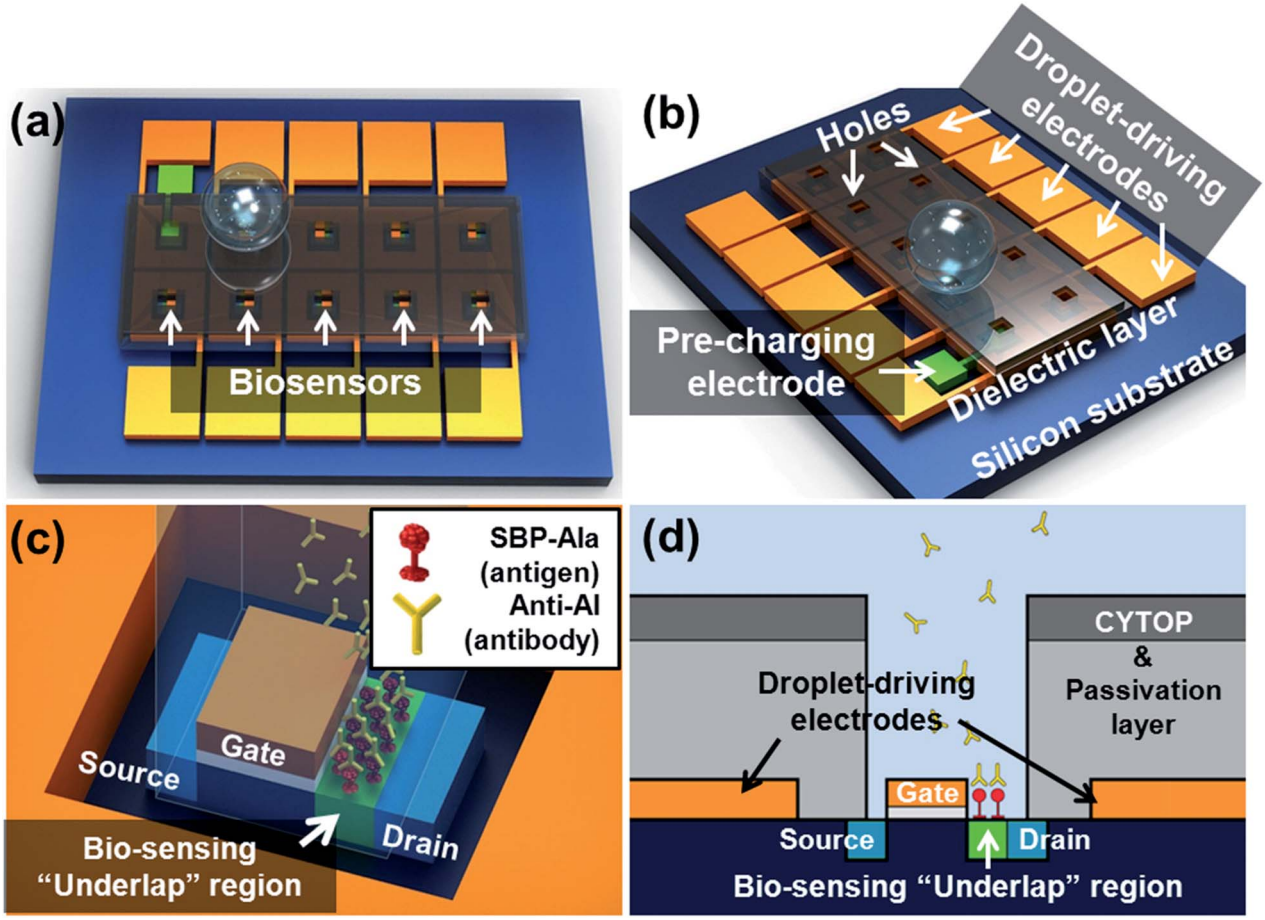

Fig. 1 Schematics of the proposed device: (a) a top-view, (b) a side-view, (c) a magnified view of the embedded underlap FET biosensor and (d) a cross-sectional view of the biosensor.

a stabilization layer to reduce the I_D fluctuation that can arise during the subsequent bio-experiment. Fig. 2(d) shows a magnified view of the underlap FET embedded in the digital microfluidic device. The figure shows the underlap region with a length of 900 nm. Annealing at 400 °C for 30 minutes by forming gas, which is a mixture of hydrogen and nitrogen, was followed to cure the interface traps at the interface of the gate oxide and the silicon channel. Finally, using a lift-off process, 40 nm thick CYTOP™ film was selectively coated onto the same region covered by the passivation layer. This makes the droplet-moving region on the droplet-driving electrodes hydrophobic, which is critical to enable EWOD actuation.

2.2 Droplet actuation

Because a single-plate structured EWOD device, which is a coplanar structure without a common ground electrode, is used here instead of the conventional double-plate EWOD device, it is possible to adopt a new droplet-driving mechanism called 'pre-charging' of the droplet.[21] This lowers the driving voltage significantly. 'Pre-charging' voltage was applied between the droplet and the droplet-driving electrode prior to EWOD actuation. This voltage is directly applied to the water droplet *via* the pre-charging electrode, which is surrounded by the droplet-driving electrode, as shown in Fig. 2(b). After the pre-charging of the droplet, a 'driving' voltage with the same magnitude but opposite polarity against the pre-charging voltage is applied to the next adjacent electrode, onto which the droplet should be moved. The droplet is then moved onto the next electrode by the electrostatic attractive force between the droplet and the next electrode. Pre-charging and driving voltages of 20 V were used for transport and merging of the sample droplets, which were in this case deionized (DI) water, phosphate-buffered saline (PBS), anti-AI solution and anti-rabbit IgG solution.

2.3 Bio-experimental sequence

To draw the target molecules, the probe molecules should be immobilized on the underlap region so that the underlap FET can function as a biosensor. Here, SBP-AIa and anti-AI are used as the probe and the target material, respectively. SBP-AIa is immobilized according to the same method described in the literature[20] before the subsequent bio-experiments with the digital microfluidic device (see the ESI document†).

Using the aforementioned digital microfluidic operations, a PBS droplet enclosing 0.00005% (w/v) Pluronic F127 (Sigma-Aldrich) is introduced onto the underlap FET. The hydrophobicity of the CYTOP™ film on the droplet-driving electrodes can be diminished by the bio-molecules in the droplet. Thus, the Pluronic F127 is enclosed in all sample droplets as an additive

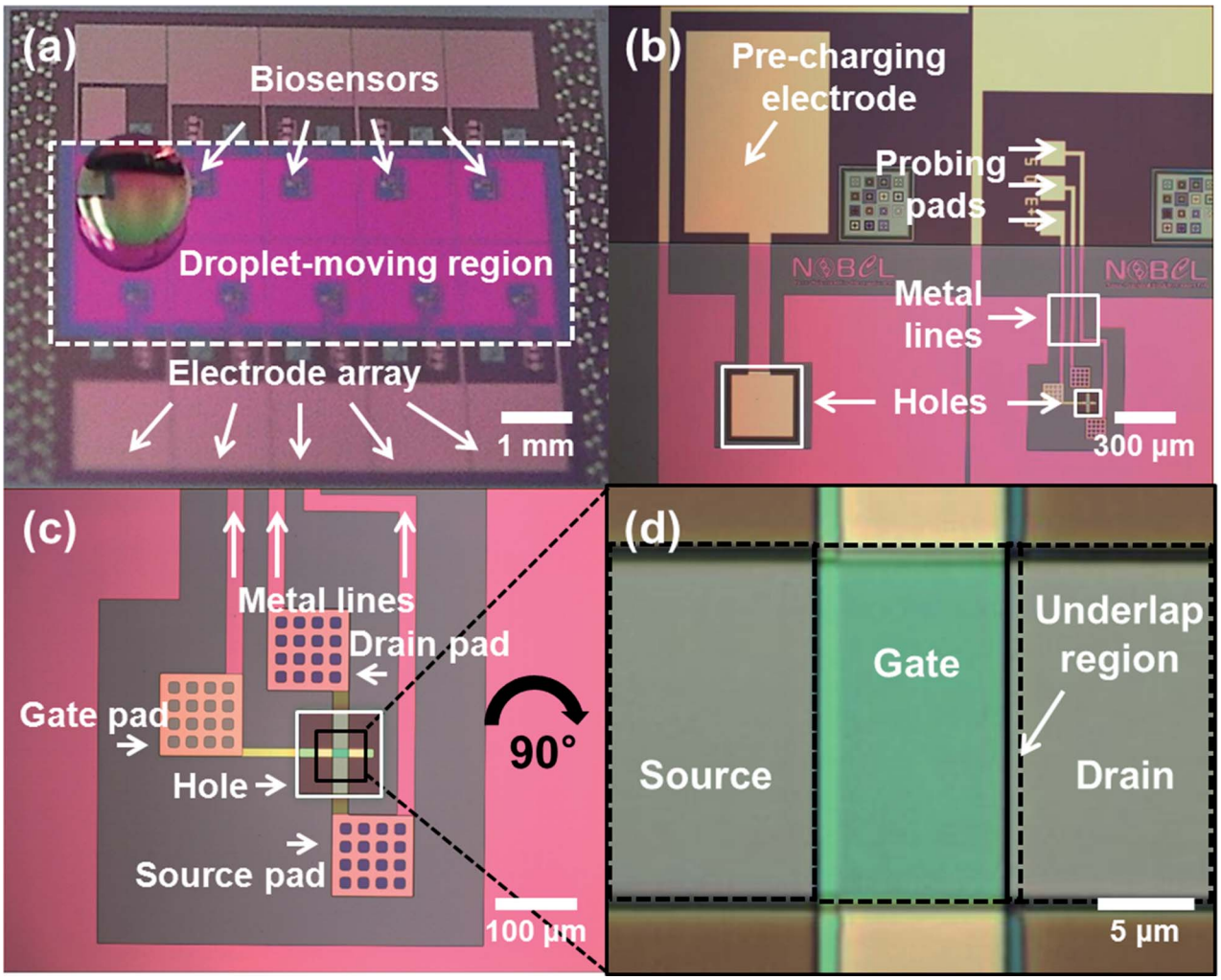

Fig. 2 Microscopic images of the fabricated device: (a) an overall view of the device with a droplet on it, (b), (c) a magnified view of the components required for the operation of the device and (d) a magnified view of the underlap FET biosensor.

which sustains the hydrophobicity. Using an Agilent 4156C precision semiconductor parameter analyzer, the I_D value of the underlap FET biosensor is measured at one-second intervals with a gate bias of 0.7 V (the subthreshold region of the underlap FET) and a drain bias of 0.05 V (Fig. 3(a) and (b)). When the I_D value is stabilized, another bio-molecular sample droplet including anti-AI or anti-rabbit IgG and 0.00005% (w/v) Pluronic F127 is introduced, pre-charged, and driven to the electrode until it encounters the pre-existing PBS droplet, as shown in Fig. 3(c) and (d). The I_D value is continually traced until it no longer changes after the two droplets are merged. The PBS droplet containing Pluronic F127 is placed on the underlap FET to cancel out any possible noise that can arise from the existence of the Pluronic F127 by equating its concentration in the PBS droplet and that in the anti-AI or anti-rabbit IgG sample droplet.

3. Results and discussion

3.1 Droplet actuation

Droplets of DI water, PBS, anti-AI solution and anti-rabbit IgG solution with a volume of 2.5 μL were transported *via* a pre-charging method with a driving voltage of 20 V (see the ESI, Fig. S1†). It was found that EWOD actuation was inhibited by the lack of hydrophobicity of the CYTOP™ film after the introduction of anti-AI and anti-rabbit IgG sample droplets on the film surface. To avoid this problem, Pluronic F127 was added to anti-AI and anti-rabbit IgG solutions following the process outlined in previous reports.[22,23] Thus, the anti-AI and anti-rabbit IgG sample droplets were successfully moved onto the digital microfluidic device.

The merging of the PBS droplet with Pluronic F127 and the anti-AI with Pluronic F127 is achieved by EWOD actuation with a pre-charging method (see the ESI, Fig. S2†).

3.2 Detection of anti-AI bio-molecules

In the first bio-experiment, the droplets of the anti-rabbit IgG sample and the anti-AI sample were added sequentially to determine that the drain current would significantly change only when the anti-AI sample was added. As shown in Fig. 4(a), a PBS droplet with Pluronic F127 was placed on an underlap FET biosensor and the initial level of I_D was then measured. The length of the underlap region for the biosensor used in this

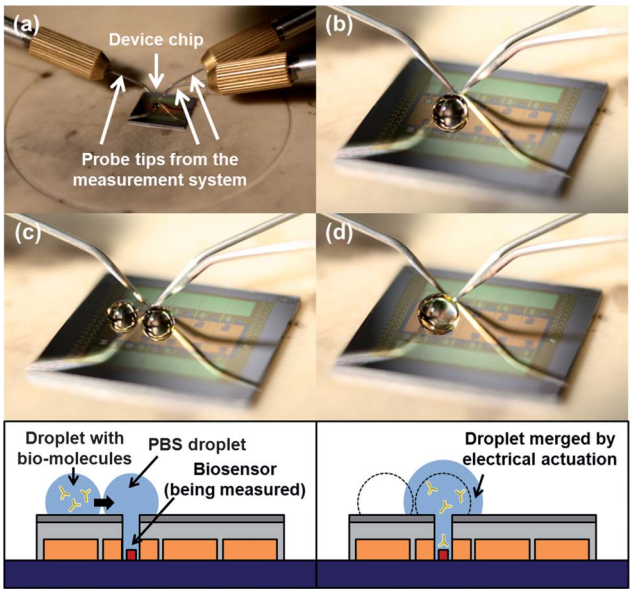

Fig. 3 Experimental set-up and sequence: (a) a device chip is put on a probe station with three probing tips touching the probing pads of a biosensor; (b) a PBS droplet is introduced onto the SBP-AIa immobilized biosensor and the drain current is measured; (c) a bio-molecular sample droplet is put on the device; and (d) the bio-molecular sample droplet is merged into the PBS droplet on the biosensor.

experiment was 900 nm. After the stabilization of I_D at $\sim 10^{-7}$ A, a droplet of the anti-rabbit IgG sample with a concentration of 10 μg ml^{-1} was merged into the PBS droplet to note the effect of non-specific binding. Because there are no target molecules in the anti-rabbit IgG sample that specifically bind to SBP-AIa, the I_D remained nearly unchanged, as expected. However, when the anti-AI sample droplet with a concentration of 10 μg ml^{-1} (133 nM) was merged into the PBS-and-anti-rabbit IgG-merged droplet, I_D decreased significantly and abruptly from approximately 10^{-7} A to 10^{-11} A. This 10^4-fold current reduction can assure a wide sensing window and thus guarantees high sensitivity.

In the previous experiment, the anti-rabbit IgG sample and anti-AI sample droplets were merged sequentially to determine whether the reduction of the I_D was caused by the specific binding between the SBP-AIa and the anti-AI. However, there was a concern that anti-rabbit IgG can unwantedly modify the SBP-AIa-coated underlap surface and influence the binding between the SBP-AIa and the anti-AI molecules. Thus, a merging experiment was independently conducted on different chips with the same device configuration. Bio-experiments with anti-rabbit IgG (10 μg ml^{-1}) and anti-AI (10 μg ml^{-1}) samples on two separate biosensors were conducted. As shown in Fig. 4(b), there is a considerable decrement of I_D in the anti-AI sample droplet, whereas there is no change of I_D in the anti-rabbit IgG sample droplet. It was concluded that the change in I_D arises wholly from the specific binding between SBP-AIa and anti-AI.

3.3 Detection limit of the underlap FET biosensor

It is important to investigate the limit of detection (LOD) in a sensor device. By changing anti-AI concentration from 0.5 fg ml^{-1} (66.7 aM) to 0.5 ng ml^{-1} (66.7 pM), the LOD was extracted. The length of the underlap region for the biosensors used in these experiments was 900 nm. Fig. 5(a) shows the ratio of the initial I_D (I_1) value to the final I_D (I_2) value when the target droplet reaches the underlap FET and I_D is stabilized. Because I_D is reduced when the anti-AI molecules attach to the SBP-AI molecules, the (I_1/I_2) ratio is always larger than unity. As more anti-AI molecules attach to the SBP-AI molecules, I_D is reduced further. As Fig. 5(a) shows, the lowest LOD was found to be 0.5 pg ml^{-1} (6.67 fM). Below this LOD, I_D is no longer changed by

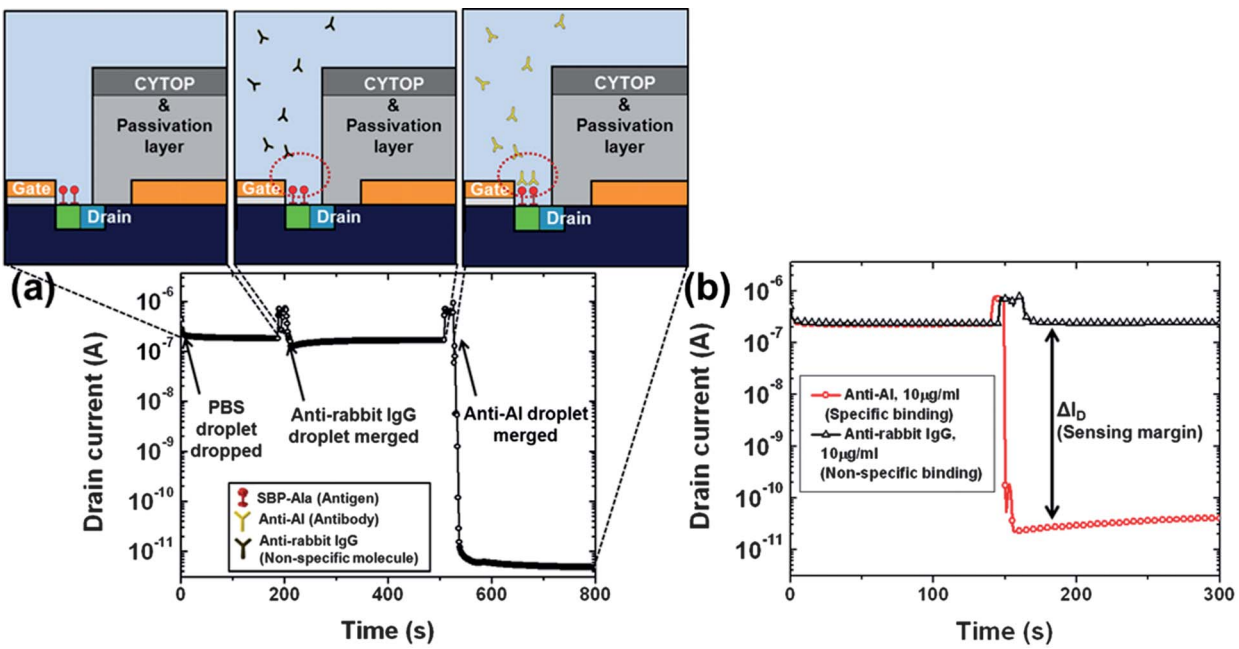

Fig. 4 (a) Measured drain current when droplets of anti-rabbit IgG and anti-AI solution were sequentially merged into a PBS droplet. (b) Two separate experimental results are acquired when each droplet of anti-rabbit IgG and anti-AI solution is merged into a PBS droplet.

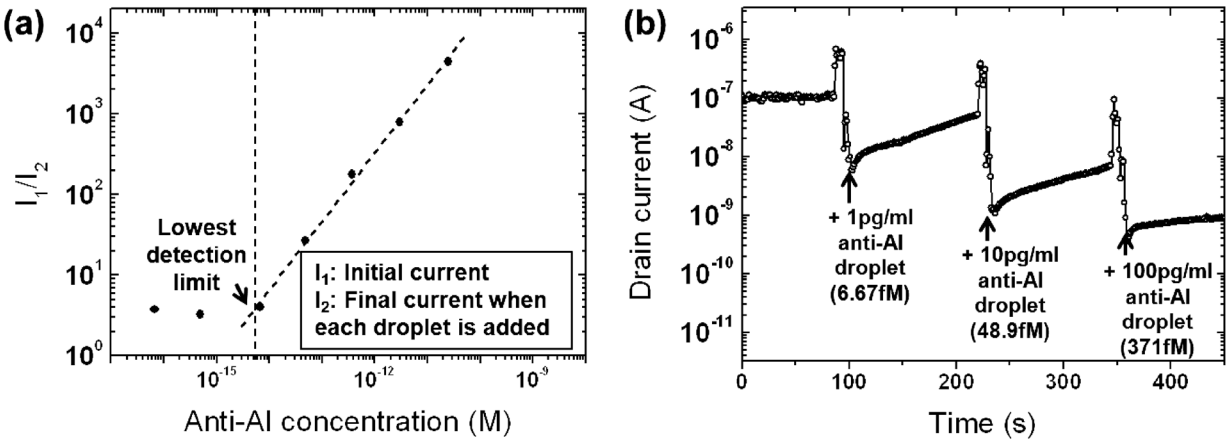

Fig. 5 (a) Ratio of the initial current to the current which is acquired when anti-AI droplets of different concentrations were added. (b) Measured drain current when anti-AI droplets of different concentrations were sequentially added.

an additional reduction in the concentration. It should be noted that there is a linear relationship between the (I_1/I_2) ratio and the concentration, which is of importance in sensor calibration.

In Fig. 5(b), the real-time experimental result for the determination of the LOD is shown. The I_D value is continually reduced as anti-AI droplets with a higher concentration are added. I_D changes within 20 seconds as each droplet of the anti-AI sample with a higher concentration was added. As multiple droplets are iteratively added to the pre-existing merged droplet, the final concentration of the droplet is increased. A droplet of PBS with Pluronic F127 was placed at first and a unit droplet of 1 pg ml^{-1} anti-AI droplet is added. As two droplets with equal volume are merged together, the net concentration of anti-AI becomes 0.5 pg ml^{-1}, which corresponds to 6.67 fM. Then, a droplet of 10 pg ml^{-1} anti-AI is merged to the pre-existing double-volume droplet additionally; the net concentration of anti-AI becomes 3.67 pg ml^{-1}, which corresponds to 48.9 fM. The same calculation applies for the following droplets. The net concentration is calculated and displayed in the parentheses in Fig. 5(b).

4. Conclusions

In this paper, a digital microfluidic device equipped with field effect transistor (FET)-based biosensors was proposed as a novel lab-on-a-chip platform. This device platform functioned as an advanced lab-on-a-chip with the capability to electrically control sample droplet movements and electrically detect a target sample without a complicated labeling process. Bio-molecular sample droplets were moved by means of actuating electrodes by applying the proper electrical biases. In addition, anti-AI molecules, which were the target molecules to detect in this work, were electrically detected with the underlap FET-based biosensor embedded in the digital microfluidic device. Due to the specific binding of the AI antibodies to the AI antigens immobilized on the biosensor surface, the drain current of the biosensor was reduced. The negative charges of the AI antibodies contributed to reducing the drain current by suppressing the formation of the electron channel in the n-channel underlap FET device. Thus, the proposed device was able to move the sample droplets as well as detect the target molecules in the droplets on a single chip through a real-time analysis. Moreover, the response of the embedded biosensors was fast enough to detect the target molecules in the droplet within a few tens of seconds. Although the proposed device still has a portability issue because of the bulky measurement system, the monolithic integration of the sensor and the digital microfluidic parts on a single substrate enables the further integration of a self-power supply system and read-out circuitry for a future all-in-one chip without any external equipment. The fabrication technology used for the proposed system is also adequate for mass production, so the fabrication cost can be lowered further. Furthermore, the proposed system would be able to detect many other molecules in a sample droplet with different probe molecules functionalized on each biosensor. Therefore, this device platform can be a useful and effective development for a future all-in-one lab-on-a-chip device to be used in point-of-care testing (POCT) and micro-total-analysis systems (μ-TAS).

Acknowledgements

This research was supported by a grant from the National Research Foundation of Korea (NRF) funded by the Korean Ministry of Education, Science and Technology (MEST) (no. 2011-0020487). It was also partially supported by the National Research and Development Program (NRDP, 2011-0002182) for the development of biomedical function monitoring biosensors.

Notes and references

1 M. Abdelgawad and A. R. Wheeler, *Adv. Mater.*, 2009, **21**, 920.
2 R. B. Fair, *Microfluid. Nanofluid.*, 2007, **3**, 245.
3 S. K. Cho, H. Moon and C.-J. Kim, *J. Microelectromech. Syst.*, 2003, **12**, 70.
4 V. Srinivasan, V. K. Pamula and R. B. Fair, *Lab Chip*, 2004, **4**, 310.
5 A. R. Wheeler, H. Moon, C. A. Bird, R. R. O. Loo, C.-J. Kim, J. A. Loo and R. L. Garrell, *Anal. Chem.*, 2005, **77**, 534.
6 Y.-H. Chang, G.-B. Lee, F.-C. Huang, Y.-Y. Chen and J.-L. Lin, *Biomed. Microdevices*, 2006, **8**, 215.
7 I. Barbulovic-Nad, S. H. Au and A. R. Wheeler, *Lab Chip*, 2010, **10**, 1536.
8 L. Malic, D. Brassard, T. Veres and M. Tabrizian, *Lab Chip*, 2010, **10**, 418.
9 L. Malic, T. Veres and M. Tabrizian, *Biosens. Bioelectron.*, 2009, **24**, 2218.
10 L. Malic, T. Veres and M. Tabrizian, *Lab Chip*, 2009, **9**, 473.

11 A. R. Wheeler, H. Moon, C.-J. Kim, J. A. Loo and R. L. Garrell, *Anal. Chem.*, 2004, **76**, 4833.
12 H. Moon, A. R. Wheeler, R. L. Garrell, J. A. Loo and C.-J. Kim, *Lab Chip*, 2006, **6**, 1213.
13 K. P. Nichols and H. J. G. E. Gardeniers, *Anal. Chem.*, 2007, **79**, 8699.
14 G. Zheng, F. Patolsky, Y. Cui, W. U. Wang and C. M. Lieber, *Nat. Biotechnol.*, 2005, **23**, 1294.
15 E. Stern, J. F. Klemic, D. A. Routenberg, P. N. Wyrembak, D. B. Turner-Evans, A. D. Hamilton, D. A. LaVan, T. M. Fahmy and M. A. Reed, *Nature*, 2007, **445**, 519.
16 H. Im, X.-J. Huang, B. Gu and Y.-K. Choi, *Nat. Nanotechnol.*, 2007, **2**, 430.
17 B. Gu, T. J. Park, J.-H. Ahn, X.-J. Huang, S. Y. Lee and Y.-K. Choi, *Small*, 2009, **5**, 2407.
18 X. P. A. Gao, G. Zhen and C. M. Lieber, *Nano Lett.*, 2010, **10**, 547.
19 J.-H. Ahn, S.-J. Choi, J.-W. Han, T. J. Park, S. Y. Lee and Y.-K. Choi, *Nano Lett.*, 2010, **10**, 2934.
20 K.-W. Lee, S.-J. Choi, J.-H. Ahn, D.-I. Moon, T. J. Park, S. Y. Lee and Y.-K. Choi, *Appl. Phys. Lett.*, 2010, **96**, 033703.
21 K. Choi, M. Im, J.-M. Choi and Y.-K. Choi, *Microfluid. Nanofluid.*, 2012, **12**, 821.
22 V. N. Luk, G. C. H. Mo and A. R. Wheeler, *Langmuir*, 2008, **24**, 6382.
23 S. H. Au, P. Kumar and A. R. Wheeler, *Langmuir*, 2011, **27**, 8586.